applied sciences

MDPI

Article

Suppressing Salt Transport through Composite Pervaporation Membranes for Brine Desalination

Lin Li [1], Jingwei Hou [1,*], Yun Ye [1], Jaleh Mansouri [1,2], Yatao Zhang [3] and Vicki Chen [1]

1 The United Nations Educational, Scientific and Cultural Organization (UNESCO) Centre for Membrane Science and Technology, School of Chemical Engineering, University of New South Wales, Sydney 2052, Australia; lin.li@student.unsw.edu.au (L.L.); yun.ye@unsw.edu.au (Y.Y.); j.mansouri@unsw.edu.au (J.M.); v.chen@unsw.edu.au (V.C.)

2 Cooperative Research Centre for Polymers, Notting Hill 3168, Australia

3 School of Chemical Engineering and Energy, Zhengzhou University, Zhengzhou 450001, China; zhangyatao@zzu.edu.cn

* Correspondence: Jingwei.hou@unsw.edu.au

Received: 30 June 2017; Accepted: 16 August 2017; Published: 19 August 2017

Featured Application: The pervaporation membranes fabricated in this study can be potentially used for brine treatment.

Abstract: Pervaporation membranes have gained renewed interest in challenging feedwaters desalination, such as reverse osmosis (RO) concentrated brine wastewater. In this study, composite polyvinyl alcohol (PVA)/polyvinylidene fluoride (PVDF) pervaporation membranes were prepared for brine treatment. The composite membrane was firstly studied by adjusting the cross-linking density of PVA by glutaraldehyde: the membrane with higher cross-linking density exhibited much higher salt rejection efficiency for long-term operation. A trace of salt on the permeate side was found to diffuse through the membrane in the form of hydrated ions, following solution-diffusion mechanism. To further suppress the salt transport and achieve long-term stable operation, graphene oxide (GO) was incorporated into the PVA layer: the addition of GO had minor effects on water permeation but significantly suppressed the salt passage, compared to the pure PVA/PVDF membranes. In terms of brine wastewater containing organic/inorganic foulant, improved anti-fouling performance was also observed with GO-containing membranes. Furthermore, the highest flux of 28 L/m^{2}h was obtained for the membrane with 0.1 wt. % of GO using 100 g/L NaCl as the feed at 65 °C by optimising the pervaporation rig, with permeate conductivity below 1.2 μS/cm over 24 h (equivalent to a salt rejection of >99.99%).

Keywords: brine wastewater treatment; pervaporation; composite PVA/PVDF membrane; graphene oxide; anti-fouling properties

1. Introduction

Desalination has been widely utilized to relieve the shortage of fresh water in many parts of the world. However, a large amount of brine wastewater is also produced as a by-product of desalination. For example, seawater reverse osmosis (RO) retentate may contain concentrated salt, humic acid and other dissolved solids. The disposal of brine wastewater into the ocean or inland could lead to environmental and ecological problems [1]. Due to high osmotic pressures, RO cannot be utilized to treat such wastewater. On the other hand, the treatment efficiency of thermally driven processes like membrane distillation (MD) is less dependent on the feed solution concentration, and can be regarded as a promising candidate in brine wastewater treatment [2,3]. However, the major problems for the industrial application of MD are membrane fouling/scaling and pore wetting.

More recently, to address the pore wetting, a dense hydrophilic pervaporation membrane has been explored for brine treatment. Pervaporation is also a thermally driven process, and the main water transport mechanism is solution-diffusion [4]. It has been extensively studied for organic dehydration [5,6]. The purpose of both desalination and organic solvents dehydration is to separate water from the bulk feed solution; however, feed properties vary significantly. For organic solvent dehydration, water usually only accounts for less than 10% of the bulk solution [7], while water is the major component in feed for desalination (more than 90%). Thus, the major problem of applying many conventional pervaporation membranes for desalination is that the membranes are not stable in the solution with both high water fractions and elevated temperatures.

Polyvinyl alcohol (PVA) pervaporation membranes have high water vapor permeability, satisfactory membrane-forming capability and excellent anti-fouling property. Recently, PVA membranes have been applied for pervaporation desalination, but a certain amount of salt can still diffuse through the polymeric layers in the form of hydrated salt ions [8,9]. This unfavorable effect can be partially mitigated by polymer cross-linking. However, a higher salt rejection would be always compromised by a reduced permeability [10,11]. Aside from the organic cross-linker, the addition of inorganic nanofillers can also enhance the stability of the composite pervaporation membranes. For example, the PVA/maleic acid/silica freestanding membranes exhibited a reduced swelling degree with higher silica concentration [12,13]. Furthermore, graphene oxide (GO), a unique 2D inorganic material, has good interfacial compatibility with PVA due to the formation of hydrogen bonds [14], showing good potential to enhance PVA stability. GO has been extensively investigated for gas and liquid separation membranes [15,16]. For porous filtration membranes, the incorporation of GO can improve the permeation flux, salt rejection and anti-fouling properties due to improved hydrophilicity [17–23]. For a porous hydrophobic membrane for MD desalination applications, the immobilization of GO by PVDF as the binder material on the surface of polytetrafluoroethylene (PTFE) membranes showed enhanced flux due to selective sorption, nanocapillary effect, reduced temperature polarization and polar functional groups in GO [24]. It can also improve the thermal, mechanical and electrical properties of the composite membranes [25,26]. Considering its 2D structure, the incorporation of GO can potentially suppress the passage of hydrated salt ions within the PVA polymer. In addition, stacked GO laminates can also form highly efficient molecular sieving channels within polymeric matrix [27,28]. However, these aspects have yet to be explored for pervaporation membranes.

Furthermore, most studies on pervaporation desalination so far only use single monovalent salt solutions as feed, and the systems are only evaluated for a relatively short period. The long-term performance of composite pervaporation membranes is crucial for evaluating their feasibility for practical application, especially for complex brine treatment. Thus, in this study, a series of composite PVA/PVDF membranes were fabricated by coating a thin layer of PVA onto commercial hydrophobic PVDF membranes. Different cross-linking density was investigated to understand their effect on the membrane performance. In addition, GO nanosheets were blended into the PVA layer to further suppress salt transport through the membrane. To better understand the properties of the GO/PVA composite membrane, freestanding GO/PVA membranes were fabricated to investigate the interactions between GO and PVA, as well as the water/salt diffusion process within the composite layer. Furthermore, the composite membrane's anti-fouling performance was explored using highly concentrated brine solutions containing humic and calcium salts. Lastly, the pervaporation rig optimization was carried out to promote the operational flux for the composite membranes.

2. Materials and Methods

2.1. Materials

Commercial hydrophobic microfiltration PVDF flat sheet membrane (Millipore, GVHP 0.22 μm, and thickness 125 μm, Billerica, MA, USA) was used in this study. Polyvinyl alcohol (PVA, Mw 89k–98k, 99+ % hydrolysed) was purchased from Sigma-Aldrich (Sigma-Aldrich Corp., St. Louis, MO, USA).

Sodium chloride (NaCl) and potassium hydroxide (KOH) pellets were supplied by Ajax Finechem (Cheltenham, VIC, Australia). Dextran (Mw 9k–11k) and glutaraldehyde (25% in water) were obtained from Alfa Aesar (Thermo Fisher Scientific, Heysham, UK). Hydrochloric acid (HCl, 32% aqueous solution) was obtained from RCl Labscan (RCl Labscan Limited, Bangkok, Thailand). Graphene oxide nanosheets were fabricated from graphene with a modified Hummer's method. The detailed process can be found in our previous publication [28].

2.2. Composite Membrane Preparation

The commercial supporting membrane was firstly pre-treated with 1 M KOH solution at 65 °C water bath for different length (0.5, 1, 2, 6 and 8 h) [29,30]. The KOH treatment led to reduction in water contact angle due to the hydrophilization effect. In this work, 2 h pre-treatment time was selected as longer treatment time did not lead to the increase of surface hydrophilicity (Figure S1). Subsequently, the membrane was rinsed with Milli-Q water and dried at room temperature. For the casting solution, aqueous PVA solution (10 wt. %) was prepared by dissolving PVA powder in Milli-Q water at 80 °C water bath with mechanical stirring for at least 6 h. Then the PVA solution was cooled down to room temperature. A certain amount of glutaraldehyde, and quencher methanol were added to the aqueous PVA solution and the mixture was magnetically stirred for another 30 min, which was followed by the addition of catalyst HCl and stirring for another 5 min. The molar ratio of glutaraldehyde/PVA repeat unit (denoted as MR value) was varied, while the ratio of methanol/HCl/PVA was maintained invariant, i.e., 1 g PVA was mixed with 2 mL of 10% methanol and 0.4 mL of 1 M HCl. To prepare the composite membrane with MR value of 0.2, for 1 g PVA prepared for the casting solution, the glutaraldehyde used (25% in water) was 1.72 mL. The PVA concentration in the final casting solution was maintained at 5 wt. % by adjusting the amount of Milli-Q water in the casting solution. The casting machine (Sheen 1133N automatic film applicator, Sheen Instruments, Surry, UK) was used to cast the PVA membrane on PVDF supports with a casting speed of 50 mm/s under 50% humidity. Then the coated membrane was dried at room temperature overnight, followed by oven drying at 80 °C for 30 min.

For the GO-containing PVA composite membrane fabrication, a certain amount of GO was evenly dispersed into the PVA casting solution containing glutaraldehyde and methanol. To initiate the cross-linking, HCl was then added to the above casting solution and stirred for 5 min. The membrane casting and drying procedures are identical to the previous pure PVA composite membranes. The weight ratio of GO to PVA (0.1, 0.2, 0.3 wt. %) was used to denote different samples, e.g., PVA0.1GO/PVDF denoted composite membrane with 0.1 wt. % of GO in PVA matrix. For the PVA-GO composite membranes, the molar ratio of glutaraldehyde to PVA repeat unit was kept invariant of 0.2.

In order to understand the interfacial interactions between GO and PVA, the freestanding PVA-GO membranes were prepared by pouring the above-mentioned casting solution in Petri dishes, followed by the same drying and post-heat treatment procedure as the cast coated membrane.

2.3. Pervaporation Desalination

Pervaporation desalination experiments were conducted by using a laboratory scale pervaporation unit, shown in Figure 1 A membrane with an effective surface area of 40 cm^2 was placed in the middle of the module, where four thermocouples were installed to monitor the inlet and outlet temperature of feed and permeate, in order to have an accurate measurement of the temperature difference on both feed and permeate sides across the membrane. During the pervaporation test, the feed solution was preheated in a water bath and pumped to the membrane module with a cross-flow velocity (CFV) of 0.625 m/s, while maintaining feed inlet temperature to the module at 65 ± 1 °C. The permeate water vapor was withdrawn by a pump on the permeate side with vacuum pressure around 24 kPa (unless otherwise stated), and collected in the beaker on the balance after condensing (cold water maintained at ~10 °C). Both the feed pump and permeate pump used in this experiment were Masterflex L/S

variable speed digital peristaltic pump (Cole-Parmer, Vernon Hills, USA). Spacers (commercial RO module spacer, with filament thickness of 0.66 mm, mesh length of 3.1 mm and spacer thickness of 1.18 mm, Synderfiltration, Vacaville, USA) were used in both of the membrane feed and permeate sides to support the membrane. During the operation, the feed tank was topped up using the solution with the same concentration as the original feed.

The salt rejection (R) was calculated by the following equation:

$$R = \frac{C_f - C_p}{C_f} \times 100\% = \frac{\kappa_f - \kappa_p}{\kappa_f} \times 100\% \quad (1)$$

where C_f and C_p referred to the feed and permeate salt concentration, κ_f and κ_p referred to the feed and permeate conductivity.

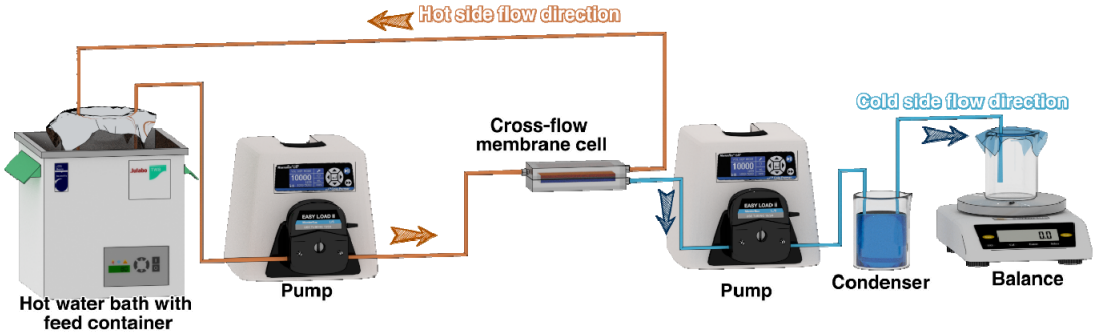

Figure 1. Schematic diagram of cross-flow pervaporation setup with flat-sheet membrane module.

2.4. Membrane Characterization

2.4.1. Scanning Electron Microscopy (SEM)

The surface and cross-section of the membranes were characterized by field emission scanning electron microscopy (FE-SEM, FEI Nova NanoSEM, Hillsboro, OR, USA). The cross-sectional SEM images of the composite membrane were obtained by snapping the membrane in liquid nitrogen. Samples for FE-SEM were prepared by sputter coating a thin layer of chromium under vacuum to generate conductivity. The qualitative surface chemistry of the membrane after desalination was investigated by energy dispersive X-ray spectroscopy (EDX) (FEI Nova NanoSEM and Hitachi S3400, Hitachi Ltd, Tokyo, Japan) to detect the presence of salt.

2.4.2. Membrane Hydrophobicity/Hydrophilicity Characterization

Static contact angles were measured using a contact angle goniometer (KSV CAM 200, Biolin Scientific, Gothenburg, Sweden) by the sessile drop method. Reported values were the average of at least 5 measurements.

2.4.3. Equilibrium Water Content (EWC)

EWC was measured to assess the cross-linked PVA's swelling property, as the ratio of the weight of water in the hydrogel to the weight of the hydrogel at equilibrium hydration. A freestanding hydrogel film was weighted and then immersed in 50 mL Milli-Q water for at least 24 h at room temperature, in order to achieve the equilibrium hydration state. The surface of the film was then blotted with an absorbent tissue paper (Kimwipe, Holcomb Bridge Road Roswell, GA, Canada) to remove excess water present on the surface and weighed again. The EWC value was calculated as follows:

$$EWC = \frac{m_w - m_d}{m_w} \quad (2)$$

where m_w and m_d represented the weight of cross-linked PVA at equilibrium hydration and dry state.

2.4.4. Salt Desorption Test

Salt transport in hydrogel film was measured using kinetic desorption experiment at room temperature. Dense freestanding membrane was prepared following the same procedure as for the EWC test. A hydrogel film with known thickness was immersed in 50 mL of 100 g/L NaCl for 24 h, which was long enough for the film to absorb an equilibrium amount of NaCl from the solution. Then the surface of the film was dried by Kimwipe and placed in a beaker with 50 mL Milli-Q water and stirred by magnetic stirring at around 500 rpm speed. Solution conductivity increased as the salt diffused out of the film into the Milli-Q water and the solution conductivity was recorded. Calculation of the NaCl diffusivity in the hydrogels was done using a Fickian analyses of NaCl desorption from a planar film.

2.4.5. Pore size Characterization

Liquid entry pressure (LEP) and mean pore size of the composite membrane were measured using capillary flow porometer from Porous Materials Inc. (PMI, Ithaca, NY, USA), based on wet/dry flow method [31]. A membrane sample with a diameter of 13 mm was placed in the chamber between two O-rings. In addition, then the membrane surface was covered by the wetting agent (Galwick®, PMI, Ithaca, NY, USA) with defined surface tension (15.9 dynes/cm). The gas flow rate through the membrane was measured as a function of the differential pressure. All porometry tests were performed at room temperature.

2.4.6. Pressurized Dead-End Filtration Test

For the membrane pore size smaller than the porometer instrument capability, a pressurized filtration test was used to determine the membrane pore size with a dead-end filtration membrane cell. Membrane resistance and permeability were also investigated using the same technique. Before the test, membrane sample was soaked in Milli-Q water overnight. Permeate flux over time was monitored with different feed solutions, i.e., Milli-Q water, 30 g/L NaCl, and 100 mg/L dextran. In addition, the dextran content of both feed and permeate was measured using the total organic carbon analyser (TOC, Shimadzu V-CSH, Kyoto, Japan). The entire filtration test was performed at room temperature.

2.4.7. X-ray Diffraction (XRD)

To determine whether GO sheets were dispersed as separated sheets in PVA matrix, XRD measurements (Empyrean X-ray diffraction system, PANalytical, 7602 EA Almelo, the Netherlands) was carried out by using Cu K_α radiation.

2.4.8. Fourier Transform Infrared Spectroscopy (FT-IR)

FT-IR (Spotlight 400, PerkinElmer, Waltham, MA, USA) was used to characterize the surface properties of composite membranes.

2.4.9. Differential Scanning Calorimetry (DSC)

Thermal analysis of the freestanding membrane was conducted using a DSC Q20 (TA Instruments, Inc., New Castle, DE, USA). The samples were heated from −30 °C to 300 °C at a rate of 10 °C/min in a nitrogen atmosphere. Approximately 6–8 mg of sample is used for each DSC measurement.

3. Results

3.1. Investigation on Cross-linking of PVA by Glutaraldehyde

3.1.1. Pervaporation Performance Using Single Salt Brine

PVA/PVDF membranes fabricated with different molar ratio of glutaraldehyde to PVA repeat unit (MR values of 0.025, 0.1, 0.2) were investigated regarding their pervaporation desalination performance using 100 g/L NaCl as the feed (Figure 2). In this work, each pervaporation test was carried out with at least two membrane samples, and the difference in permeation flux and salt rejection was less than 10% throughout the whole testing process.

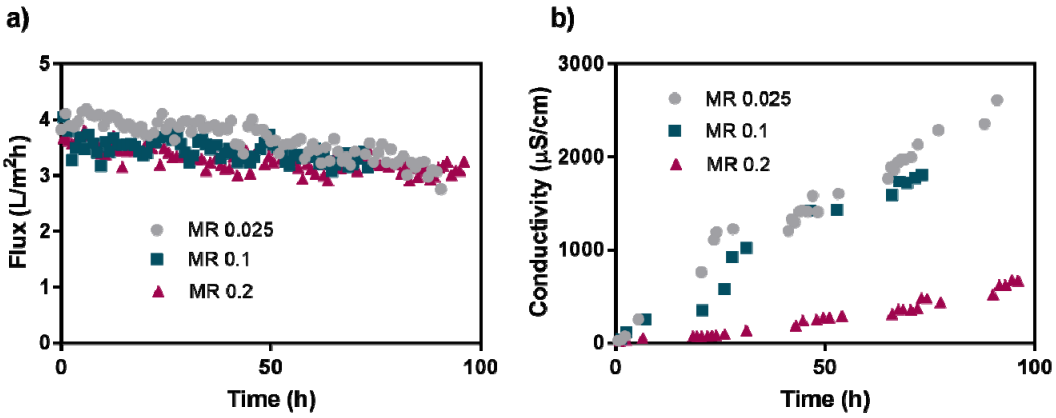

Figure 2. (**a**) Flux and (**b**) permeate conductivity profile of composite PVA/PVDF membrane with different molar ratio of glutaraldehyde to PVA repeat unit (MR 0.025, 0.1, 0.2) using a feed solution of 100 g/L NaCl at 65 °C.

As shown in Figure 2a, all membrane samples had comparable water flux under the same operating condition although a slightly lower flux was observed for membranes with higher MR value. Besides, all the membranes experienced continuous flux declines during the whole testing process due to the gradual increase of the feed concentration. In terms of the permeate conductivity, all membrane samples showed an increased conductivity with a longer operation time, and the membrane with the highest MR value (0.2) showed the most stable salt rejection after 96 h operation. This trend suggested that the cross-linking of PVA can benefit the operational stability of the membrane, which can be attributed to more acetal/ether linkages with higher MR value, leading to the improved structural stability with reduced free volume and swelling tendency [32,33]. Comparatively, the virgin supporting membrane, hydrophobic PVDF membrane with nominal pore size of 0.22 µm, showed a permeate conductivity of 2 mS/cm after 10 min of operation under the same operating condition. This indicated that the salt rejection efficiency of the pervaporation process was not attributed to the supporting membrane used in the composite membrane.

The water flux results in this work were comparable to the values reported in previous literatures of pervaporation membranes, when taking the operating temperature and feed solution properties into consideration. For example, composite membranes containing 100–1000 nm PVA surface coating on polysulfone membrane yielded fluxes of 4.6–7.4 L/m^{2}h with 30 g/L NaCl solution at 70 °C [34]. In another line of research, a slightly higher water flux (5.57 L/m^{2}h) was obtained with a PVA/polyacrylonitrile (PAN)/polyethylenimine (PEI) triple-layered membrane when using 50 g/L NaCl solution as feed under room temperature [35]. In terms of the salt rejection, the PVA membrane in this work exhibited higher salt rejections even with more concentrated feed solution compared with the literatures [34,35].We also explored the membrane stability by recycling the membrane and testing the membrane using different feed concentrations and salt types, as shown in Figures S2 and S3.

However, considering the permeate flux was relatively invariant, the gradual increase of permeate conductivity for all the PVA/PVDF membranes indicated a more rapid transport of salt ions as the pervaporation test proceeded. The following characterizations and discussion were aimed to better understand the transport mechanism of salt through the composite PVA/PVDF membrane, to provide guidance for the further modification of such membranes.

3.1.2. Transport Mechanism of Salt

The salt transport through the membrane was further confirmed by the EDX results (Figure 3): the presence of salt crystals was observed on the membrane feed side as well as within the porous substrate after 96 h pervaporation test. The transport of salt ions through the PVA layer could be originated via the free volume between PVA polymeric chains. In this work, the gradual increase of the conductivity suggested a change of PVA chain structure overtime, possibly due to the swelling effect by hot water feed during the pervaporation process.

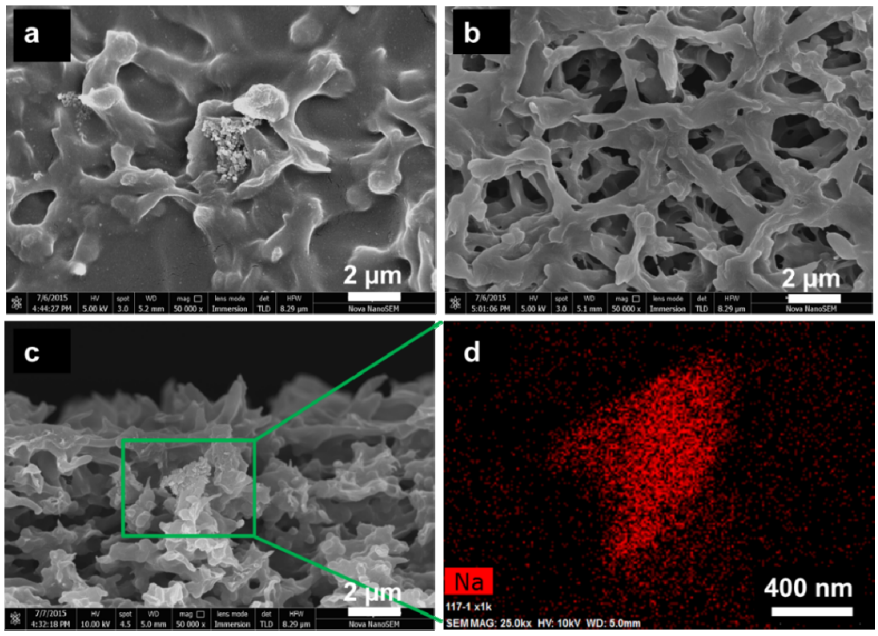

Figure 3. SEM and EDX autopsy of the composite membrane after 96 h pervaporation test (membrane with MR of 0.2). (**a**) Feed side, (**b**) permeate side and (**c**) cross-section of the composite membrane; and (**d**) EDX mapping the membrane cross-section beneath the PVA coating layer.

To further explore the PVA membrane pore structure, a porometer test was carried out with the composite membrane (both fresh membranes and membranes after 96 h permeation test) using Galwick as a wetting agent at room temperature. However, no direct liquid penetration through the membrane was observed for all the membranes with different MR values under maximum feed of 10 bar. To further explore the pore size (free volume) range of the composite membrane, we conducted the dead-end filtration test with 15 bar feed pressure using fresh composite membranes at room temperature. As suggested in Table 1, the resistance for MR 0.2 membrane was in the range of RO membranes, with a pure water flux of 1.4 ± 0.4 L/m^{2}h. The rejection of dextran (1–2 nm) can remain ~83.4% over 10 h operation. In comparison, the rejection of NaCl (diameter of hydrated Na^+ 0.716 nm, hydrated Cl^- 0.664 nm) was much lower at around 33%, which was lower than the reported PVA composite nanofiltration (NF) membrane [36,37]. Thus, it was believed that the pore size (free volume) of the composite membrane (MR of 0.2) was in the range of NF membrane (below 1 nm). Deng et al. also reported that the diameter of casted/cross-linked PVA membrane's free volume was around 0.426 nm tested by bulk positron annihilation lifetime spectroscopy (PALS) [38].

Table 1. Pressurized filtration test results of composite PVA/PVDF membrane using feed solutions of Milli-Q water, 30 g/L NaCl or 100 mg/L dextran, under TMP of 15 bar at room temperature. The flux was recorded after the stabilization of 30 min. The membrane resistance (R_m) was calculated based on $R_m = \frac{\Delta P}{\mu J}$, where ΔP, μ and J indicated the trans-membrane pressure, viscosity of Milli-Q water and corresponded pure water flux, respectively.

Pressurized Filtration Test Results	Unit	Commercial PVDF	MR0.025	MR0.1	MR0.2
Pure water flux	L/m^2h	>15,000	240 ± 56	5.5 ± 0.27	1.4 ± 0.4
Permeability	L/m^2 h·bar	>1000	16 ± 3.5	0.37 ± 0.018	0.093 ± 0.027
Average membrane resistance	m^{-1}	$<3.9 \times 10^{11}$	$\sim 2.5 \times 10^{13}$	$\sim 1.1 \times 10^{15}$	4.3×10^{15}
Flux using 30 g/L NaCl as the feed	L/m^2h	/	129 ± 16.5	3.74 ± 0.23	0.54 ± 0.1
Salt rejection using 30 g/L NaCl as the feed	%	/	~0	~9	~33
Flux using 100 mg/L Dextran as the feed	L/m^2h	/	142 ± 21	4.69 ± 0.42	0.99 ± 0.18
Rejection using 100 mg/L Dextran as the feed	%	/	~0	53.9%	83.4

It also indicated that the change of MR value had a significant effect on the PVA layer pore (free volume) structure. With the increase of MR value, the membrane resistance gradually increased, accompanied with the increase of rejections for salt ions and dextran. In this work, the lowest resistance was observed for the membrane with MR 0.025: it fell into the range of UF or even MF membranes.

Figure 4 showed the SEM and atomic force microscope (AFM) analysis of membrane with different MRs. With the increase of MR value, the PVA layer thickness became more homogeneous, accompanied with the loss of surface roughness. The surface roughness of PVDF membrane after KOH pre-treatment was ~200 nm, which was comparable to the composite membrane with MR of 0.025. This indicated that the coating of PVA with low MR value (0.025) did not significantly change the membrane's surface roughness. Furthermore, the change of MR value did not only alter the membrane pore (free volume) structure; it can also affect the chemical component within the selective layer. Theoretically, the cross-linking of PVA with glutaraldehyde can consume the hydroxyl groups for the polymer. It can also increase the polymer chain structure rigidity. Both aspects can lead to the reduced EWC value for the membrane as shown in Table 2, which well aligns other studies [32,33].

Table 2. Characterization results of composite PVA/PVDF membrane (Diffusivity of NaCl in pure water is 14.7×10^{-6} cm^2/s). MR: Molar Ratio. EWC: Equilibrium Water Content.

Composite Membrane	Surface Roughness (nm)	EWC (%) in Water	EWC (%) in 100 g/L NaCl	NaCl Diffusivity (10^{-6} cm^2/s)
MR0.025	281.5 ± 7.78	184.5 ± 35.3	129.7 ± 16.8	2.02 ± 0.97
MR0.1	140 ± 31.1	60.4 ± 5.2	56.6 ± 2.5	1.42 ± 0.36
MR0.2	106.4 ± 13.58	49.6 ± 7.0	38.1 ± 6.3	0.64 ± 0.13

This could well explain the observation of slightly lower permeate flux but improved salt rejection for the membrane with higher MR values (Figure 2): the transport rate of bulkier penetrant (hydrated salt ions) was more sensitive to the changes in free volume than those of smaller penetrant (water vapor) [39,40]. Therefore, the decreased diffusivity of salt through the membrane with higher MR (Table 2) can be attributed to its lower free volume.

During the pervaporation process, salt ions could diffuse through the PVA layer in the form of hydrated ions and condensed together with water due to the temperature drop in the permeate side. The increase of cross-linking density can retard but not completely block the passage of salt ions. At the same time, the gradual up-take of water can lead to the swelling of PVA due to the preferable adsorption of water molecules by the hydroxyl groups on PVA chains. In the swollen PVA especially the one with large free volume, more water was adsorbed by the hydroxyl groups of PVA chains, where a small fraction of hydrated salt ions could fit into such enlarged free volume, allowing their gradual passage. As a result, the increased free volume allows fast dissolution and diffusion of bulkier hydrated salt ions through the membrane [34,41,42], which explained the gradual

loss of the salt rejection during the extended pervaporation test (Figure 5). Thus, in the following session, GO nanosheets, impermeable hydrophilic nanosheets, were incorporated into the PVA matrix to limit the free volume increase with time in PVA layer and further suppress salt transport through the membrane. MR value of 0.2 was applied to fabricate the membranes with GO because of its highest salt rejection efficiency compared to membranes with lower MR values.

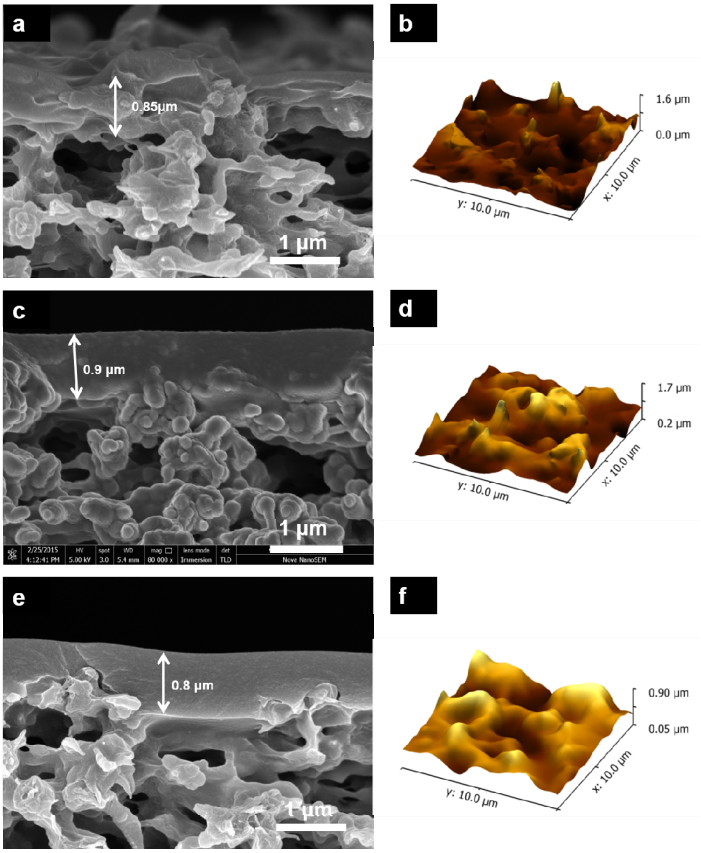

Figure 4. Cross-sectional SEM and AFM surface height images of PVA/PVDF composite membrane with MR of (**a**) and (**b**) 0.025; (**c**) and (**d**) 0.1; (**e**) and (**f**) 0.2.

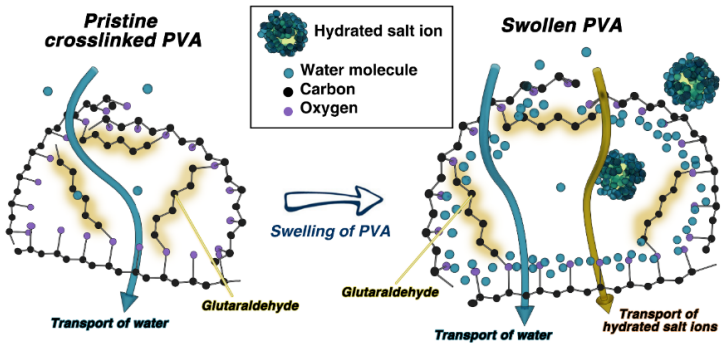

Figure 5. Schematic diagram of salt passage through the swollen PVA membrane (not to scale).

3.2. Incorporation of GO into PVA Matrix

3.2.1. Characterizations

The addition of a small amount of GO into PVA formed small protrusions on the membrane surface, and this became more significant with the increase of GO loading within the coating layer

(Figure 6). Similar surface morphology was observed after incorporating GO into polyether block amide (Pebax) matrix using cast coating method [43]. In terms of the cross-sectional images (Figure S4), they showed good agreement with the surface SEM images. The pure PVA coating was even with a thickness of around 0.8 μm. The incorporation of GO reduced the smoothness for the PVA-GO coating layer, especially when the GO loading was relatively high. During the formation of PVA-GO surface coating, the gradual evaporation of the solvent (water) allowed the cross-linking of the PVA chains, forming the final coating layer of 0.5–1 μm. In terms of the GO, the evaporation-induced capillary flow during the drying process, together with the viscous PVA solution, disrupted the entropy-driven phase transition of GO, leading to the formation of surface protrusions [44].

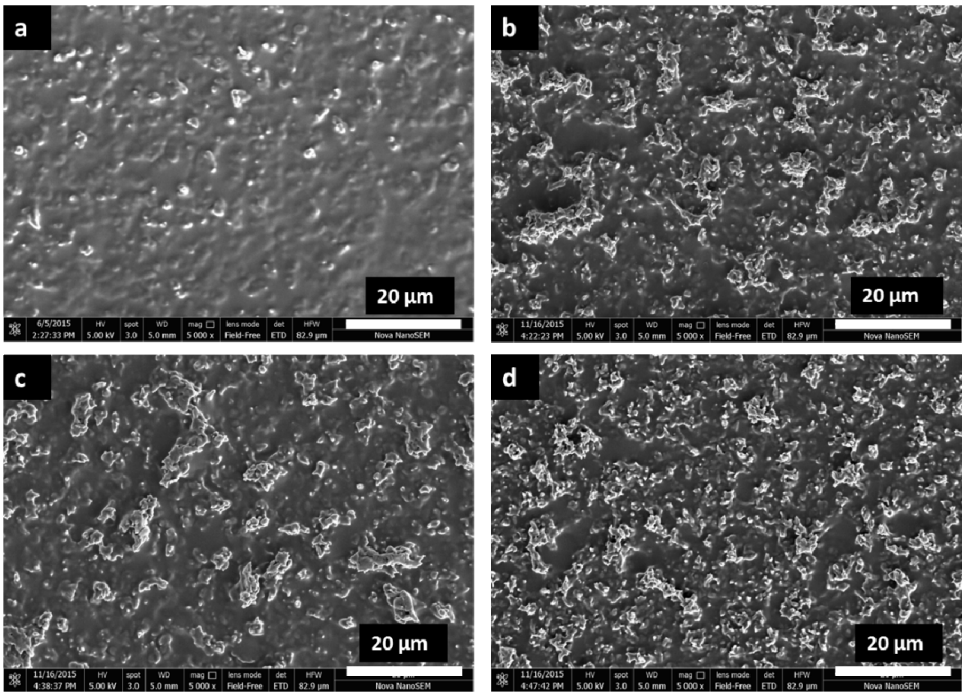

Figure 6. Surface SEM images of composite membranes fabricated with cast coating method: (**a**) pure PVA coating; and PVA-GO hybrid coating with (**b**) 0.1 wt. %, (**c**) 0.2 wt. %, (**d**) 0.3 wt. % GO loading.

The XRD pattern can reveal the GO nanosheets arrangement within the hybrid coating layer. As shown in Figure 7, for the pure GO coated membrane, it had a clear peak at 10.6°, suggesting the GO nanosheets were piled together with an average interlayer distance of 0.83 nm. After incorporating the GO into PVA matrix, no clear GO peak can be observed. This observation was in good agreement with the previous researches [14,45]. This can be attributed to the good interfacial compatibility between GO and PVA: the presence of carboxyl groups and hydroxyl groups on GO can form hydrogen bonding with hydroxyl groups on PVA. As a result, the GO nanosheets can be well dispersed within the PVA matrix at the molecular level [26].

The successful incorporation of GO was further evidenced by the FT-IR patterns, as shown in Figure 8 The characteristic peaks of GO powder at around 3280 cm^{-1} and 1725 cm^{-1} corresponded to O–H and C=O stretch, which indicated the existence of hydroxyl groups and carbonyl groups on GO. Besides, the peak at around 2950 cm^{-1} confirmed a large amount of C–H stretch on GO. Compared to pure PVA coating, the emerging peaks for the PVA-GO composite coating layer at the region of 3100–3010 cm^{-1} can be ascribed to alkenyl C–H stretch due to the presence of GO. In addition, the right shift of the O-H stretching peaks were detected with the addition of GO in PVA matrix (from 3375 cm^{-1} for pure PVA to 3345 cm^{-1} for PVA with GO of 0.3 wt. %). This observation confirmed the formation

of hydrogen bonding between hydroxyl/carboxylate groups on GO and hydroxyl groups on PVA chains, which was consistent with those of other studies [14,45,46].

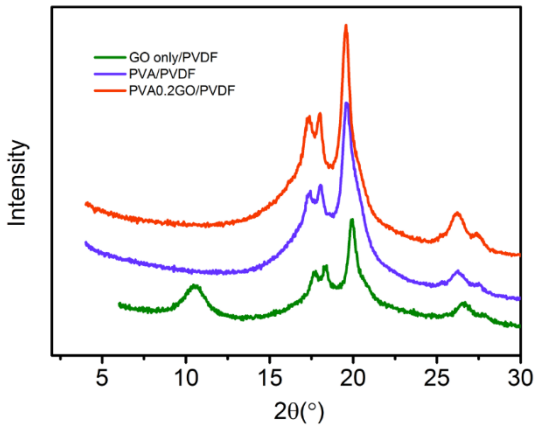

Figure 7. XRD curves of composite membranes.

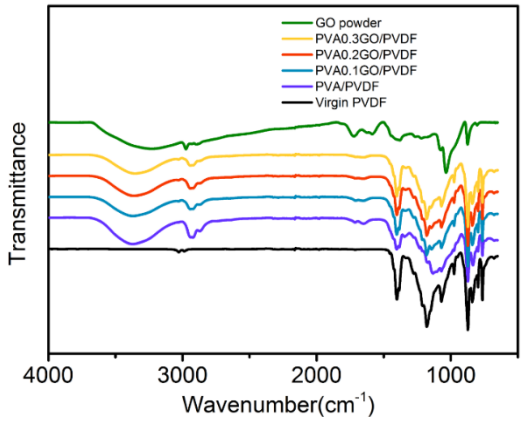

Figure 8. FT-IR curves of PVA-GO/PVDF membranes with GO loading of 0.1, 0.2 and 0.3 wt. %.

Regarding the contact angle shown in Table S1, the addition of GO into PVA matrix slightly increased the contact angle of the membrane surface. For example, the pure PVA surface coating has a contact angle of 30.2 ± 3.5°, compared with the 37.1 ± 2.3° for the composite membrane containing 0.2 wt. % GO. This can be attributed to the presence of a large amount non-polar benzene rings on GO surface, as well as the formation of hierarchical surface morphology after the addition of GO [47].

To better understand the effect of GO incorporation on the coating layer properties, freestanding PVA-GO films were also prepared and characterized to explore their surface morphology, thermal and swelling properties. The thickness of the freestanding films was around 100 μm. From the digital photo (Figure S5), with higher GO loading, the freestanding film color changed from almost transparent to yellowish brown. Similar to the composite membrane fabricated via cast coating, the addition of GO introduced wrinkles and protrusions onto the membrane surface, as shown in Figure S6. As the freestanding films were fabricated via the solvent evaporation method, without the shear force induced alignment during the casting process, the GO nanosheets randomly oriented within the original membrane casting solution, and eventually led to the wrinkled paper-like structure on the surface due to the capillary flow during the solvent evaporation process. Based on the SEM images, GO was homogeneously dispersed within the PVA matrix. Same as the composite membranes, no GO peak was observed in freestanding films after the incorporation of GO in PVA matrix from the

XRD patterns (Figure S7), indicating a good interfacial compatibility between the GO nanosheets and the PVA matrix.

As shown in Table 3, the DSC results exhibited an increased Tg for the freestanding films after the incorporation of GO nanosheets (from around 48 °C to around 60 °C). This further confirmed the formation of hydrogen bonding between GO nanosheets and PVA matrix, which reduced the polymer chain mobility. This could be also lead to the rigidification of polymer chains near the GO sheets [15]. Similar trends were also observed by incorporating a small amount of GO into PVA matrix [45,48].

Table 3. Thermal and swelling property of the freestanding films (PVA0.1GO denoted membrane with 0.1 wt. % of GO in PVA matrix). PVA: polyvinyl alcohol. GO: graphene oxide.

Freestanding Films	Tg (°C)	EWC in Milli-Q Water (%)	EWC in 100 g/L NaCl (%)	NaCl Diffusivity (10^{-6} cm^2/s)
PVA only	48	49.6 ± 7	38.1 ± 6.3	0.64 ± 0.13
PVA0.1GO	59	25.35 ± 1.41	28.06 ± 1.07	0.712 ± 0.001
PVA0.2GO	60	38.15 ± 2.05	34.98 ± 1.66	0.549 ± 0.066
PVA0.3GO	60	35.35 ± 4.37	30.68 ± 0.54	0.526 ± 0.005

The freestanding films' swelling properties were also studied as it is closely related to the membrane's cross-linking density and free volume [12]. The equilibrium water content (EWC) values of freestanding films (Table 3) in both Mill-Q water and 100 g/L NaCl aqueous solution were investigated. Among different membranes, the pure PVA freestanding film exhibited the highest EWC values for both Milli-Q water and salt water. The initial addition of GO (0.1 wt. %) significantly reduced the EWC value. This can be attributed to the impermeable feature of GO and formation of hydrogen bonding between GO and PVA, which reduced the solubility of water in the PVA polymer chains. However, with the increase of GO loading (0.2 and 0.3 wt. %), the EWC values increased again due to the water adsorption on the nanosheet surface, but they were still lower than the pure PVA films. Another potential reason could be the aggregation of GO sheets in PVA matrix created new pathways for water adsorption and diffusion. Smaller free volume fraction was also obtained by adding GO into PVA matrix from other studies [45].

By comparing the EWC value in Milli-Q water and salt water, it was found that for pure PVA films the EWC value in salt water was significantly lower than that in Milli-Q water. While for the films with GO incorporated, the difference is less significant. This indicated that the swelling ability of PVA with GO was less affected by the salt content, compared to pure PVA. Furthermore, with the addition of GO into the PVA matrix, the salt diffusivity tended to decrease. This was caused by much longer and more torturous transport pathways for salt to pass through the film, since GO is an impermeable nanosheet to salt ions. It is worth mentioning that in the salt diffusivity test, with the addition of GO, the amount of salt absorbed by the membrane decreases significantly. After immersing the hydrated films into Milli-Q water, the equilibrium solution conductivity dropped from around 120 μS/cm for pure PVA films down to 20 μS/cm for PVA with 0.1 wt. % GO. It took similar time (~200 s) for both films to achieve equilibrium during the immersion process. This clearly indicates that less salt is adsorbed by the membrane with GO incorporated: i.e., the GO incorporation considerably decreased the membrane's salt solubility in the PVA films.

From the above characterizations on both composite membranes and freestanding films with GO incorporated into PVA matrix, a good dispersion of GO in PVA was observed by SEM and XRD results; and the hydrogen bonding formed between PVA and GO is detected from FT-IR and DSC analysis. The EWC and NaCl diffusivity results showed that the incorporation of impermeable GO decreased the size of the free volume in PVA matrix and also the water and salt solubility in the matrix.

3.2.2. Pervaporation Performance Using Single Salt Brine

The composite membranes with different GO loadings in PVA matrix (0.1, 0.2, and 0.3 wt. %) were tested in the pervaporation setup, which was then compared with the pure PVA/PVDF membrane (MR value of 0.2). For each membrane, Milli-Q water permeation tests were firstly conducted for at least 4 h. Compared with pure PVA/PVDF membrane, the incorporation of 0.1 wt. % GO showed the negligible effect on the Milli-Q water flux (4.38 L/m^{2}h). However, further increase of the GO loading can lead to a marginal loss of the flux: 94.4 and 85.5% of the original PVA/PVDF flux can be obtained for composite membranes containing 0.2 and 0.3 wt. % GO (results not shown). In highly cross-linked PVA polymer chains, the free volume was organized in a tortuous manner, which led to the random and non-directional water passage pathway [49]. After the addition of GO, the presence of a large amount of hydrophobic aromatic rings on its surface can facilitate the rapid "sliding" of water molecules along its surface [50]. This aspect would facilitate the water transport through the membrane. On the other hand, the incorporation of impermeable GO sheets also increased the transport pathway length of water vapor. Meanwhile, lower free volume, measured as the EWC value, was obtained as a result of hydrogen bonding between GO and PVA chains. As a result, the initial addition of GO (0.1 wt. %) had a negligible effect on the Milli-Q water flux and a further increase of the GO loading (0.2 and 0.3 wt. %) slightly reduced the permeation flux.

In terms of the brine desalination tests with 100 g/L NaCl solution, similar flux profiles (Figure 9) were observed as to the Milli-Q results: the initial addition of 0.1 wt. % GO had a negligible effect on the brine solution flux, and a further increase of the GO loading can lead to more obvious loss of the permeation flux. In terms of permeate conductivity, it constantly increased to over 650 μS/cm (salt rejection of over 99.6%) after 96 h operation for the pure PVA/PVDF membrane, while the composite membrane containing 0.1 wt. % GO had a much more stable performance: the permeate conductivity gradually increased to less than 150 μS/cm (salt rejection of over 99.9%) for 120 h operation while maintaining lower than 50 μS/cm in the first 50 h. As discussed above, the presence of GO nanosheets within the PVA matrix can facilitate the selective water molecule transport along with its "slippery" surface, which suppressed the transport of salt ions through the composite membrane. The reduced free volume of PVA matrix had a more significant blocking effect on the larger hydrated salt ions compared with smaller water molecules. As a result, the addition of GO can improve the salt rejection for the composite membrane.

When 0.2 wt. % GO was added into the PVA matrix, the permeate conductivity was more stable (less than 30 μS/cm in 82 h operation). However, in this case, the permeate flux was much lower than the PVA0.1GO/PVDF membrane, and a significant flux decline was observed after 10 h operation. Due to the reduced free volume after GO addition, the blockage effect by the hydrated salt ions to the smaller water molecules can be more significant. This can also explain the more significant flux loss for membrane containing 0.3 wt. % GO. In addition, for the membrane containing 0.3 wt. % GO, the permeate conductivity increased more rapidly compared with a membrane containing 0.1 and 0.2 wt. % GO. The possible reason was that some defects or cracks may exist due to strong filler interactions and agglomerations. Similar results were also observed with a composite membrane containing silica nanoparticles and ordered mesoporous carbon (OMC), less water uptake and permeable flux were detected with higher loading of nanoparticles in the thin-film layer, and the overdose of nanofillers can also lead to the loss of membrane selectivity [51–53].

Upon the completion of the long-term brine desalination test, the membranes were re-tested with Milli-Q water to investigate their permeation flux recovery. The results suggested even though the initial flux was much lower, it can gradually recover to the original Milli-Q water flux prior to the brine desalination test in less than 2 h, shown in Figure S8. This observation confirmed flux decline during the brine desalination test was mainly due to the blockage of water transport pathway by the bulkier hydrated salt ions. In all, with the increase of GO loading in PVA matrix, the water flux tended to decrease for both Milli-Q water and brine, while the salt rejection firstly increased

then decreased. Similar membrane behavior has been reported for the PVA-GO-based composite pervaporation membrane for organic solution dehydration [54].

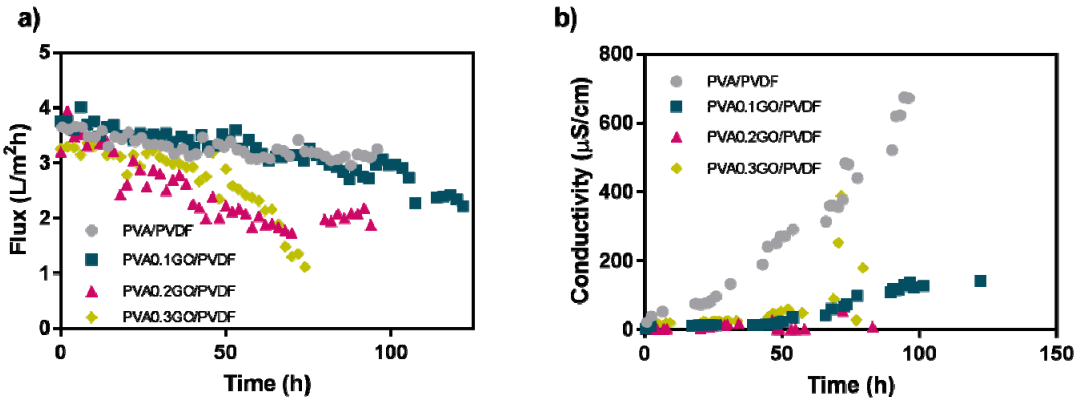

Figure 9. (**a**) Flux and (**b**) permeate conductivity profiles of the composite membrane using a feed solution of 100 g/L NaCl at 65 °C.

3.3. Anti-Fouling Performance

GO nanosheets are known to improve the anti-fouling property for the mixed matrix filtration membranes [18,20–23]. This is ascribed to the improved membrane's hydrophilicity due to the hydrophilic groups on GO. However, whether GO can promote the anti-fouling performance of pervaporation membranes has not been explored yet. The fouling study on pure PVA/PVDF composite membranes (Figure 10) showed that the presence of 10 mg/L humic acid in 100 g/L NaCl aqueous solution had a negligible effect on the flux, but increased the permeate conductivity significantly (from 370 μS/cm to 2.8 mS/cm at the end of 72 h operation). This may indicate that the attachment of humic acid on the surface of PVA layer and the binding between humic acid and salt ions accelerated the salt transport through the membrane [55]. With GO incorporated in the PVA coating layer, increased permeate conductivity was also observed (from 140 to 355 μS/cm at the end of 120 h operation), which well aligned with the membrane without GO. However, the increase was less significant. This indicated that the incorporation of GO in PVA matrix stabilized the composite membrane's performance when processing brine containing organic foulant (humic acid).

We further investigated the effect of $CaCl_2$ on the membrane performance by adding 1.26 g/L $CaCl_2$ in the mixture of 100 g/L NaCl and 10 mg/L humic acid: the presence of the inorganic salt ions had a negligible effect on the permeation flux. It is interesting that the presence of calcium slightly reduced the permeation conductivity for both pure PVA/PVDF and PVA-GO/PVDF composite membranes, which can be attributed to the formation of the bulkier calcium-humic complex [55]. The results showed that a much lower permeate conductivity was obtained for the composite membrane containing GO than the pure PVA/PVDF membrane, which clearly demonstrated the improved anti-fouling property for the composite membrane after the addition of GO. This observation also suggested better operational stability for the pervaporation desalination process compared with the MD process: the presence of $CaCl_2$ can lead to severe fouling and flux decline for virgin hydrophobic PVDF (flux dropping to 0 with permeate conductivity rising to 1 mS/cm at the end of 20 h' operation) and modified superhydrophobic membrane (flux dropping to 0 with permeate conductivity rising to 3 mS/cm at the end of 40 h' operation) during the vacuum MD process, as suggested by our previous work [56].

The permeate solution composition at the different operating time was analyzed by ICP when using feed solution containing 100 g/L NaCl, 10 mg/L humic acid and 1.26 g/L $CaCl_2$ with the composite membrane containing 0.1 wt. % GO (Table 4). With the progress of the pervaporation operation, the permeate conductivity increased due to the gradual diffusion of the sodium ions and

calcium ions through the membrane, and the diffusion rate of the smaller Na ions was higher than the bulkier Ca ions. In all, the incorporation of small amount of GO in PVA matrix efficiently slowed down the transport of salt ions through the membrane during the pervaporation process, although this was not completely prevented.

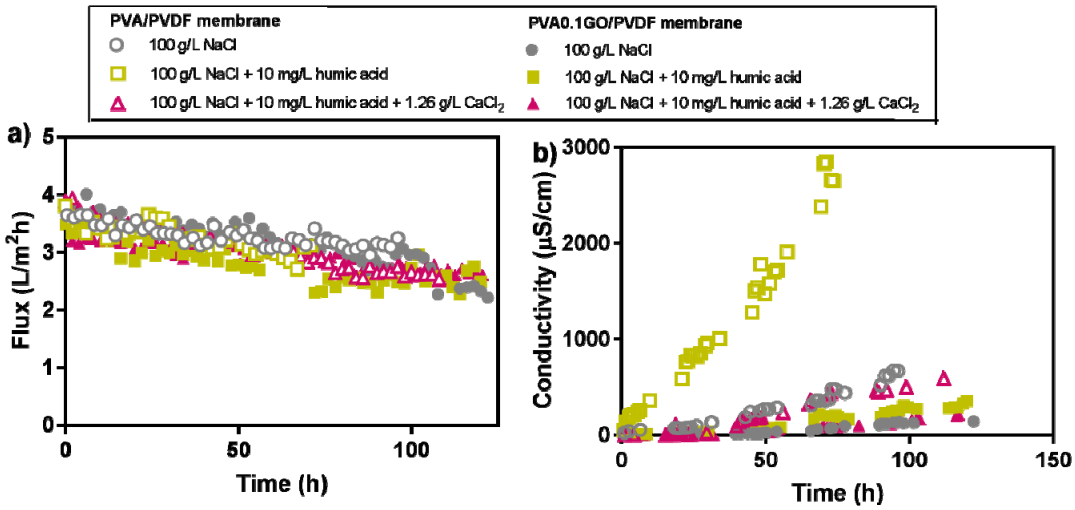

Figure 10. (**a**) Flux and (**b**) permeate conductivity profiles of the composite membrane PVA/PVDF, and PVA0.1GO/PVDF prepared by cast coating method using different feed solution.

Table 4. Permeate property of membrane PVA0.1GO/PVDF at different operation time by using feed solution of 100 g/L NaCl, 10 mg/L humic acid and 1.26 g/L $CaCl_2$, where initial feed conductivity is around 155 mS/cm, with Na^+ 39.4 g/L and Ca^{2+} 0.164 g/L.

Operation Time (h)	Conductivity (µS/cm)	Na^+ (mg/L)	Ca^{2+} (mg/L)
19.2	3.7	0.55	0.00
66.5	78.8	13.6	0.03
116.4	205	37.1	0.18
164.25	493	127	1.07

3.4. Effect of Permeate Pressure on Pervaporation Performance

As the pervaporation process is a thermal-driven process, the vapor pressure difference across the membrane plays a major role in the membrane water vapor permeability. While the main goal of this study was to suppress the salt transport through the composite membrane by modifications on PVA layer, there is still a need to suggest how the permeate pressure influenced on the membranes pervaporation performance, especially the membrane productivity. Conducting a thorough study could be an independent endeavor, however, in this study a limited number of tests were conducted to explore the effect of permeate pressure on membrane performance. A secondary condensation unit was applied next to the membrane cell in the permeate side, in order to maintain the permeate pressure at 3 kPa (instead of the initial pressure of 24 kPa). The membrane PVA/PVDF and PVA0.1GO/PVDF (both with 0.2 MR value and effective membrane area of 14.7 cm^2) were further tested, with both Milli-Q water and 100 g/L NaCl as the feeds. For the Milli-Q water feed, PVA/PVDF membrane and PVA0.1GO/PVDF membrane had very comparable flux (average flux 39.7 and 39.2 L/m^2h for 4 h operation after stabilization, results not shown). The pervaporation performance using highly concentrated NaCl as the feed was shown in Figure 11 an initial volume of 2 L feed solution with a concentration of 100 g/L was used without top-up during a 24 h operation. Both membranes showed an initial flux of 27–28 L/m^2h, which was followed by obvious flux decline (around 25%) as a result of continuously increased feed concentration. After the 24 h pervaporation test using salt water, a flux of

around 39 L/m^{2}h was restored using Milli-Q water as the feed for both membranes (results not shown). In terms of permeate conductivity, the membrane PVA0.1GO/PVDF obtained a constant value of 1–1.2 µS/cm, while the membrane PVA/PVDF showed a value of 15 µS/cm at the end of 24 h testing. This also confirmed that the addition of 0.1 wt. % GO effectively suppressed salt diffusion through the membrane. More importantly, the flux value using the same feed concentration was 9 times to that of using permeate pressure of 24 kPa. This suggested the further direction for optimization for such pervaporation wastewater treatment processes.

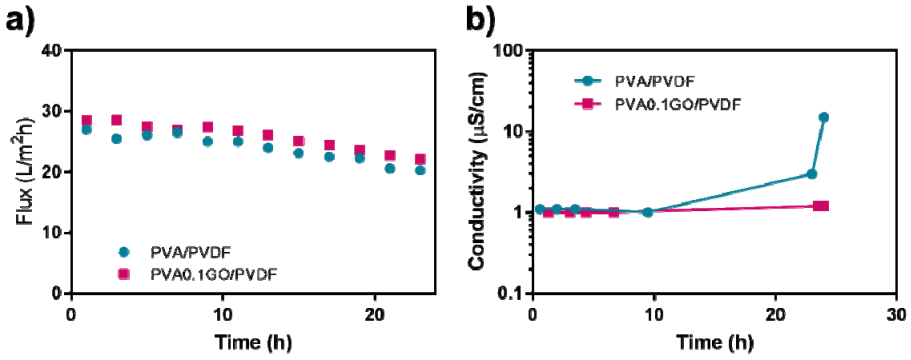

Figure 11. (**a**) Flux and (**b**) permeate conductivity profiles of composite PVA/PVDF membrane (MR value of 0.2) and PVA0.1GO/PVDF membrane using 2 L of 100 g/L NaCl as the feed without top-up at operating temperature of 65 °C.

4. Conclusions

Initially, in this work, composite membrane desalination performance was optimized by varying the cross-linking density of PVA. The results suggested the transport of salt ions through the membrane followed the solution-diffusion mechanism in the form of hydrated ions. Then, by incorporating a small amount of GO (0.1 wt. %) into PVA matrix, a high salt rejection can be maintained during the extended desalination operation, while the flux was relatively unaffected. This can be attributed to the impermeable properties of GO to salt ions and fast water molecule transport along its surface. In addition, the presence of polar groups on GO can also form hydrogen bonds with PVA, which rigidified the PVA chains and suppressed the transport of bulkier salt ions. The GO/PVA composite membrane also exhibited satisfactory anti-fouling properties during the treatment of calcium and humic-containing brine wastewater. Lastly, the study on permeate pressure indicated its crucial role in affecting the membrane productivity for such PVA-based pervaporation membranes.

Supplementary Materials: The following are available online at www.mdpi.com/2076-3417/7/8/856/s1. Figure S1: Contact angle after membrane pre-treatment, Figure S2: Flux and conductivity profile of composite PVDF membrane with KOH/MR 0.2/5 wt. % by one layer casting, where the membrane was cleaned with in-situ cleaning method: (top) "96 h 100 g/L NaCl + 24 h Milli-Q water cycle; (bottom) "23 h 100 g/L NaCl + 1 h Milli-Q water cycle". The feed inlet temperature is 65 ± 1 °C, Figure S3: Flux and conductivity profile of composite PVA/PVDF membrane with KOH/MR 0.2/5 wt. % by one layer casting using a feed solution of 30 g/L, 100 g/L NaCl and PAC solution with the same conductivity as 30 g/L NaCl (~55 mS/cm). The feed inlet temperature was 65 ± 1 °C, Figure S4: Cross-sectional SEM images of the composite membrane fabricated with the cast coating: (a,b) PVA/PVDF, (c,d) PVA0.1GO/PVDF, Figure S5: Digital photo of freestanding PVA samples with different GO loadings: (a) 0, (b) 0.1 wt. %, (c) 0.2 wt. %, and (d) 0.3 wt. %, Figure S6: SEM images of freestanding PVA membrane with GO loading of (a) 0, (b) 0.1 wt. %, (c) 0.2 wt. %, (d) magnified 0.1 wt. %, Figure S7: XRD curves of GO only/PVDF, freestanding PVA, and freestanding PVA with GO loading of 0.1 wt. %, Figure S8: Flux profile of composite membrane PVA0.1GO/PVDF using Milli-Q water, 100 g/L NaCl and Milli-Q water as the feed, sequentially, Table S1: Contact angles of the composite membrane samples with different GO loadings.

Acknowledgments: This research was supported under Australian Research Council's Discovery Projects funding scheme (DP130104048).

Author Contributions: Lin Li, Jingwei Hou and Yatao Zhang conceived the idea of suppressing salt transport by GO incorporation. The experimental work was carried out by Lin Li. Yun Ye and Jingwei Hou built the pervaporation setup. Lin Li, Jingwei Hou, Yun Ye, Jaleh Mansouri, Yatao Zhang and Vicki Chen contributed to the manuscript writing and editing.

Conflicts of Interest: The authors declare no conflict of interest.

References

1. Lattemann, S.; Höpner, T. Environmental impact and impact assessment of seawater desalination. *Desalination* **2008**, *220*, 1–15. [CrossRef]
2. Mariah, L.; Buckley, C.A.; Brouckaert, C.J.; Curcio, E.; Drioli, E.; Jaganyi, D.; Ramjugernath, D. Membrane distillation of concentrated brines—Role of water activities in the evaluation of driving force. *J. Membr. Sci.* **2006**, *280*, 937–947. [CrossRef]
3. Mericq, J.-P.; Laborie, S.; Cabassud, C. Vacuum membrane distillation of seawater reverse osmosis brines. *Water Res.* **2010**, *44*, 5260–5273. [CrossRef] [PubMed]
4. Khayet, M.; Matsuura, T. Pervaporation and vacuum membrane distillation processes: Modeling and experiments. *AIChE J.* **2004**, *50*, 1697–1712. [CrossRef]
5. Feng, X.; Huang, R.Y. Pervaporation with chitosan membranes. I. Separation of water from ethylene glycol by a chitosan/polysulfone composite membrane. *J. Membr. Sci.* **1996**, *116*, 67–76. [CrossRef]
6. Chapman, P.D.; Oliveira, T.; Livingston, A.G.; Li, K. Membranes for the dehydration of solvents by pervaporation. *J. Membr. Sci.* **2008**, *318*, 5–37. [CrossRef]
7. Shah, D.; Kissick, K.; Ghorpade, A.; Hannah, R.; Bhattacharyya, D. Pervaporation of alcohol–water and dimethylformamide–water mixtures using hydrophilic zeolite NaA membranes: Mechanisms and experimental results. *J. Membr. Sci.* **2000**, *179*, 185–205. [CrossRef]
8. Quiñones-Bolaños, E.; Zhou, H.; Soundararajan, R.; Otten, L. Water and solute transport in pervaporation hydrophilic membranes to reclaim contaminated water for micro-irrigation. *J. Membr. Sci.* **2005**, *252*, 19–28. [CrossRef]
9. Wang, Q.; Li, N.; Bolto, B.; Hoang, M.; Xie, Z. Desalination by pervaporation: A review. *Desalination* **2016**, *387*, 46–60. [CrossRef]
10. Bolto, B.; Tran, T.; Hoang, M.; Xie, Z. Crosslinked poly (vinyl alcohol) membranes. *Prog. Polym. Sci.* **2009**, *34*, 969–981. [CrossRef]
11. Praptowidodo, V.S. Influence of swelling on water transport through pva-based membrane. *J. Mol. Struct.* **2005**, *739*, 207–212. [CrossRef]
12. Xie, Z.; Hoang, M.; Duong, T.; Ng, D.; Dao, B.; Gray, S. Sol–gel derived poly (vinyl alcohol)/maleic acid/silica hybrid membrane for desalination by pervaporation. *J. Membr. Sci.* **2011**, *383*, 96–103. [CrossRef]
13. Xie, Z.; Ng, D.; Hoang, M.; Duong, T.; Gray, S. Separation of aqueous salt solution by pervaporation through hybrid organic–inorganic membrane: Effect of operating conditions. *Desalination* **2011**, *273*, 220–225. [CrossRef]
14. Huang, H.-D.; Ren, P.-G.; Chen, J.; Zhang, W.-Q.; Ji, X.; Li, Z.-M. High barrier graphene oxide nanosheet/poly (vinyl alcohol) nanocomposite films. *J. Membr. Sci.* **2012**, *409*, 156–163. [CrossRef]
15. Tan, B.; Thomas, N.L. A review of the water barrier properties of polymer/clay and polymer/graphene nanocomposites. *J. Membr. Sci.* **2016**, *514*, 595–612. [CrossRef]
16. Cui, Y.; Kundalwal, S.I.; Kumar, S. Gas barrier performance of graphene/polymer nanocomposites. *Carbon* **2016**, *98*, 313–333. [CrossRef]
17. Ganesh, B.; Isloor, A.M.; Ismail, A.F. Enhanced hydrophilicity and salt rejection study of graphene oxide-polysulfone mixed matrix membrane. *Desalination* **2013**, *313*, 199–207. [CrossRef]
18. Zinadini, S.; Zinatizadeh, A.A.; Rahimi, M.; Vatanpour, V.; Zangeneh, H. Preparation of a novel antifouling mixed matrix pes membrane by embedding graphene oxide nanoplates. *J. Membr. Sci.* **2014**, *453*, 292–301. [CrossRef]
19. Yin, J.; Zhu, G.; Deng, B. Graphene oxide (GO) enhanced polyamide (PA) thin-film nanocomposite (TFN) membrane for water purification. *Desalination* **2016**, *379*, 93–101. [CrossRef]
20. Bano, S.; Mahmood, A.; Kim, S.-J.; Lee, K.-H. Graphene oxide modified polyamide nanofiltration membrane with improved flux and antifouling properties. *J. Mater. Chem. A* **2015**, *3*, 2065–2071. [CrossRef]

21. Zhao, H.; Wu, L.; Zhou, Z.; Zhang, L.; Chen, H. Improving the antifouling property of polysulfone ultrafiltration membrane by incorporation of isocyanate-treated graphene oxide. *Phys. Chem. Chem. Phys.* **2013**, *15*, 9084–9092. [CrossRef] [PubMed]
22. Wu, H.; Tang, B.; Wu, P. Development of novel SiO_2–GO nanohybrid/polysulfone membrane with enhanced performance. *J. Membr. Sci.* **2014**, *451*, 94–102. [CrossRef]
23. Zhao, C.; Xu, X.; Chen, J.; Yang, F. Effect of graphene oxide concentration on the morphologies and antifouling properties of pvdf ultrafiltration membranes. *J. Environ. Chem. Eng.* **2013**, *1*, 349–354. [CrossRef]
24. Bhadra, M.; Roy, S.; Mitra, S. Desalination across a graphene oxide membrane via direct contact membrane distillation. *Desalination* **2016**, *378*, 37–43. [CrossRef]
25. Yin, J.; Deng, B. Polymer-matrix nanocomposite membranes for water treatment. *J. Membr. Sci.* **2015**, *479*, 256–275. [CrossRef]
26. Yang, H.-C.; Hou, J.; Chen, V.; Xu, Z.-K. Surface and interface engineering for organic–inorganic composite membranes. *J. Mater. Chem. A* **2016**, *4*, 9716–9729. [CrossRef]
27. Shen, J.; Liu, G.; Huang, K.; Jin, W.; Lee, K.-R.; Xu, N. Membranes with fast and selective gas-transport channels of laminar graphene oxide for efficient CO_2 capture. *Angew. Chem. Int. Ed.* **2015**, *54*, 578–582.
28. Zhang, Y.; Shen, Q.; Hou, J.; Sutrisna, P.D.; Chen, V. Shear-aligned graphene oxide laminate/pebax ultrathin composite hollow fiber membranes using a facile dip-coating approach. *J. Mater. Chem. A* **2017**, *5*, 7732–7737. [CrossRef]
29. Liang, B.; Zhan, W.; Qi, G.; Nan, Q.; Liu, Y.; Lin, S.; Cao, B.; Pan, K. High performance graphene oxide/polyacrylonitrile composite pervaporation membranes for desalination applications. *J. Mater. Chem. A* **2015**. [CrossRef]
30. Li, X.; Chen, Y.; Hu, X.; Zhang, Y.; Hu, L. Desalination of dye solution utilizing PVA/PVDF hollow fiber composite membrane modified with TiO_2 nanoparticles. *J. Membr. Sci.* **2014**, *471*, 118–129. [CrossRef]
31. Li, L.; Hashaikeh, R.; Arafat, H.A. Development of eco-efficient micro-porous membranes via electrospinning and annealing of poly (lactic acid). *J. Membr. Sci.* **2013**, *436*, 57–67. [CrossRef]
32. Kim, K.-J.; Lee, S.-B.; Han, N.W. Effects of the degree of crosslinking on properties of poly (vinyl alcohol) membranes. *Polym. J.* **1993**, *25*, 1295–1302. [CrossRef]
33. Zhang, L.; Yu, P.; Luo, Y. Dehydration of caprolactam–water mixtures through cross-linked pva composite pervaporation membranes. *J. Membr. Sci.* **2007**, *306*, 93–102. [CrossRef]
34. Chaudhri, S.G.; Rajai, B.H.; Singh, P.S. Preparation of ultra-thin poly (vinyl alcohol) membranes supported on polysulfone hollow fiber and their application for production of pure water from seawater. *Desalination* **2015**, *367*, 272–284. [CrossRef]
35. Liang, B.; Pan, K.; Li, L.; Giannelis, E.P.; Cao, B. High performance hydrophilic pervaporation composite membranes for water desalination. *Desalination* **2014**, *347*, 199–206. [CrossRef]
36. Peng, F.; Huang, X.; Jawor, A.; Hoek, E.M. Transport, structural, and interfacial properties of poly (vinyl alcohol)–polysulfone composite nanofiltration membranes. *J. Membr. Sci.* **2010**, *353*, 169–176. [CrossRef]
37. Baroña, G.N.B.; Choi, M.; Jung, B. High permeate flux of PVA/PSf thin film composite nanofiltration membrane with aluminosilicate single-walled nanotubes. *J. Colloid Interface Sci.* **2012**, *386*, 189–197. [CrossRef] [PubMed]
38. Deng, Y.H.; Chen, J.T.; Chang, C.H.; Liao, K.S.; Tung, K.L.; Price, W.E.; Yamauchi, Y.; Wu, K.C.W. A drying-free, water-based process for fabricating mixed-matrix membranes with outstanding pervaporation performance. *Angew. Chem. Int. Ed.* **2016**, *55*, 12793–12796. [CrossRef] [PubMed]
39. Ju, H.; Sagle, A.C.; Freeman, B.D.; Mardel, J.I.; Hill, A.J. Characterization of sodium chloride and water transport in crosslinked poly (ethylene oxide) hydrogels. *J. Membr. Sci.* **2010**, *358*, 131–141. [CrossRef]
40. Xie, Z. *Hybrid Organic-Inorganic Pervaporation Membranes for Desalination*; Victoria University: Toronto, ON, Canada, 2012.
41. Kusumocahyo, S.P.; Sano, K.; Sudoh, M.; Kensaka, M. Water permselectivity in the pervaporation of acetic acid–water mixture using crosslinked poly (vinyl alcohol) membranes. *Sep. Purif. Technol.* **2000**, *18*, 141–150. [CrossRef]
42. Xu, R.; Lin, P.; Zhang, Q.; Zhong, J.; Tsuru, T. Development of ethenylene-bridged organosilica membranes for desalination applications. *Ind. Eng. Chem. Res.* **2016**, *55*, 2183–2190. [CrossRef]

43. Zhao, D.; Ren, J.; Qiu, Y.; Li, H.; Hua, K.; Li, X.; Deng, M. Effect of graphene oxide on the behavior of poly (amide-6-b-ethylene oxide)/graphene oxide mixed-matrix membranes in the permeation process. *J. Appl. Polym. Sci.* **2015**, *132*. [CrossRef]
44. Qin, L.; Zhao, Y.; Liu, J.; Hou, J.; Zhang, Y.; Wang, J.; Zhu, J.; Zhang, B.; Lvov, Y.; Van der Bruggen, B. Oriented clay nanotube membrane assembled on microporous polymeric substrates. *ACS Appl. Mater. Interfaces* **2016**, *8*, 34914–34923. [CrossRef] [PubMed]
45. Sharma, S.; Prakash, J.; Pujari, P. Effects of the molecular level dispersion of graphene oxide on the free volume characteristics of poly (vinyl alcohol) and its impact on the thermal and mechanical properties of their nanocomposites. *Phys. Chem. Chem. Phys.* **2015**, *17*, 29201–29209. [CrossRef] [PubMed]
46. Loryuenyong, V.; Saewong, C.; Aranchaiya, C.; Buasri, A. The improvement in mechanical and barrier properties of poly(vinyl alcohol)/graphene oxide packaging films. *Packag. Technol. Sci.* **2015**, *28*, 939–947. [CrossRef]
47. Hou, J.; Dong, G.; Ye, Y.; Chen, V. Enzymatic degradation of bisphenol-a with immobilized laccase on tio 2 sol–gel coated pvdf membrane. *J. Membr. Sci.* **2014**, *469*, 19–30. [CrossRef]
48. Liang, J.; Huang, Y.; Zhang, L.; Wang, Y.; Ma, Y.; Guo, T.; Chen, Y. Molecular-level dispersion of graphene into poly (vinyl alcohol) and effective reinforcement of their nanocomposites. *Adv. Funct. Mater.* **2009**, *19*, 2297–2302. [CrossRef]
49. Ma, H.; Burger, C.; Hsiao, B.S.; Chu, B. Highly permeable polymer membranes containing directed channels for water purification. *ACS Macro Lett.* **2012**, *1*, 723–726. [CrossRef]
50. Joshi, R.; Carbone, P.; Wang, F.-C.; Kravets, V.G.; Su, Y.; Grigorieva, I.V.; Wu, H.; Geim, A.K.; Nair, R.R. Precise and ultrafast molecular sieving through graphene oxide membranes. *Science* **2014**, *343*, 752–754. [CrossRef] [PubMed]
51. Yin, J.; Kim, E.-S.; Yang, J.; Deng, B. Fabrication of a novel thin-film nanocomposite (TFN) membrane containing MCM-41 silica nanoparticles (NPs) for water purification. *J. Membr. Sci.* **2012**, *423*, 238–246. [CrossRef]
52. Kim, E.-S.; Deng, B. Fabrication of polyamide thin-film nano-composite (PA-TFN) membrane with hydrophilized ordered mesoporous carbon (H-OMC) for water purifications. *J. Membr. Sci.* **2011**, *375*, 46–54. [CrossRef]
53. Wang, X.; Chen, X.; Yoon, K.; Fang, D.; Hsiao, B.S.; Chu, B. High flux filtration medium based on nanofibrous substrate with hydrophilic nanocomposite coating. *Environ. Sci. Technol.* **2005**, *39*, 7684–7691. [CrossRef] [PubMed]
54. Wang, N.; Ji, S.; Li, J.; Zhang, R.; Zhang, G. Poly (vinyl alcohol)–graphene oxide nanohybrid "pore-filling" membrane for pervaporation of toluene/n-heptane mixtures. *J. Membr. Sci.* **2014**, *455*, 113–120. [CrossRef]
55. Meng, S.; Ye, Y.; Mansouri, J.; Chen, V. Fouling and crystallisation behaviour of superhydrophobic nano-composite pvdf membranes in direct contact membrane distillation. *J. Membr. Sci.* **2014**, *463*, 102–112. [CrossRef]
56. Meng, S.; Ye, Y.; Mansouri, J.; Chen, V. Crystallization behavior of salts during membrane distillation with hydrophobic and superhydrophobic capillary membranes. *J. Membr. Sci.* **2015**, *473*, 165–176. [CrossRef]